# DEFORMATION AND STRESS-CHANGE MODELING AT SIERRA NEGRA VOLCANO, GALÁPAGOS, FROM ENVISAT INSAR AND GPS OBSERVATIONS

**Sigurjón Jónsson[(1)], William W. Chadwick [(2)], Michael Poland[(3)], Dennis Geist[(4)]**

*[(1)]Institute of Geophysics, ETH Zurich, Schafmattstr. 30, 8093 Zurich, Switzerland, Email: sj@erdw.ethz.ch*
*[(2)] Oregon State Univ.–NOAA, 2115 SE OSU Drive, Newport, OR 97365, USA, Email: William.W.Chadwick@noaa.gov*
*[(3)]USGS, P.O. Box 51, Hawaii National Park, HI 96718, USA, Email: mpoland@usgs.gov*
*[(4)]University of Idaho, P.O. Box 443022, Moscow, ID 83844, USA, Email: dgeist@uidaho.edu*

## ABSTRACT

We use radar interferograms and GPS observations to constrain models of magma accumulation and faulting at Sierra Negra volcano, Galápagos, during the years before its 2005 eruption. The data have shown ~5 m of pre-eruption uplift and multiple trapdoor faulting events on an intra-caldera fault system. We find the pattern of uplift to be consistent with an inflating sill at 2.2 km depth under the caldera. Our deformation modeling and stress-change calculations suggest that the inflating sill triggered faulting on an inward-dipping thrust fault and that the faulting in turn relieved the pressure within the sill. This sill-fault interaction tends to thicken the sill and limit its lateral extent within the area bounded by the fault..

## 1. INTRODUCTION

Understanding the state of stress within volcanoes and how it changes with active geophysical processes is of vital importance to assess when and where magma may erupt at the surface. Observations of volcanic deformation help to constrain parameters of models that can be used to describe these processes and calculate the resulting stress changes within the volcano. The recent activity on Sierra Negra volcano, Galápagos, along with detailed Interferometric Synthetic Aperture Radar (InSAR) and GPS measurements of its surface deformation, provide a unique opportunity to study magmatic processes and the resulting stress changes within an active basaltic volcano.

Sierra Negra volcano, located on southern Isabela Island (Fig. 1), is the most voluminous of the active volcanoes in the Galápagos, with an subaerial extent of 60 km by 40 km, and a maximum elevation of 1140 m above sea level. Its caldera is elliptically shaped (7 km × 10 km) and rather shallow, only about 100 m deep. The inner-caldera floor tilts slightly down to the east and is bounded to the west and to the south by an intra-caldera fault system (Fig. 1). The near vertical fault scarps are over 100 m high in the west where the fault system forms a prominent sinuous ridge [1]. In the south the scarps are much lower, and the ridge is subdued (Fig. 1). It has been suggested that the fault system was formed through repeating "trapdoor" faulting events, driven by magma accumulation at shallow depths [1-2]. The last eruptions at Sierra Negra took place in 1979 and 2005, and like other recent eruptions were fed by circumferential vents near the northern caldera rim. The estimated lava volumes produced by these eruptions are 0.9 km$^3$ and 0.10-0.15 km$^3$, respectively [1,3-4].

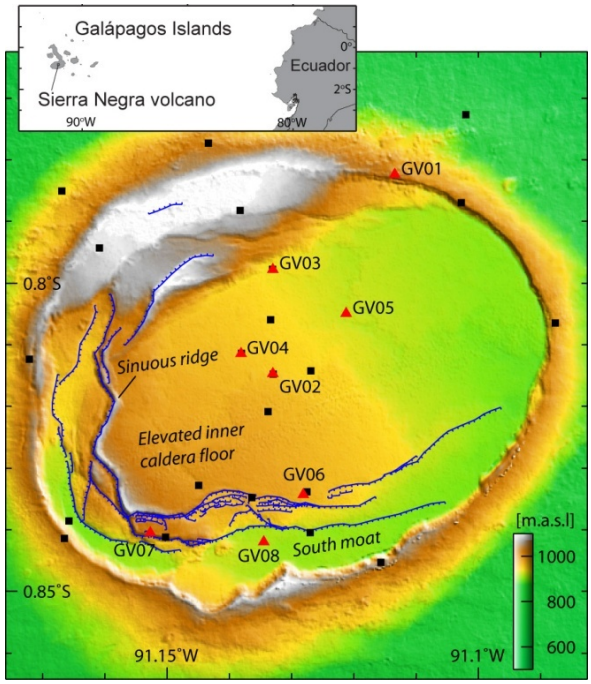


*Figure 1: Map of Sierra Negra caldera showing the intra-caldera fault system [2] and locations of campaign (black squares) and continuous (red triangles) GPS sites (GV07-08 were installed in 2006). The inset shows the location of Sierra Negra on southern Isabela Island in the Galápagos.*

Geodetic measurements of Sierra Negra during the past 15 years have revealed a remarkable sequence of events, including ~5 m of uplift prior to the 2005 eruption and repeated trapdoor faulting events on the intra-caldera fault system. InSAR observations (from 1992) and GPS measurements (from 2000) showed an approximately axisymmetric uplift pattern and variable uplift rates preceding the eruption, with a short period

*Proc. of FRINGE 2007 Workshop, Frascati, Italy, 26 – 30 November 2007*
*(ESA SP-649, February 2008)*

of subsidence in 2001-03 [5-6]. The inflation has been modeled as being due to filling and pressurization of a sill at about ~2 km depth [5-7].

Inflation prior to the 2005 eruption was punctuated by at least three faulting events on the intra-caldera fault system on Sierra Negra, in January 1998, in April 2005, and just before the eruption started on in October 2005. The first two faulting events were associated with earthquakes ($M_w$=5.0 on 11 January, 1998 [8] and $m_b$=4.6 on 16 April 2005 [9]). The 2005 eruption started after a magnitude $M_w$=5.5 earthquake on 22 October [9], when a large part of the intra-caldera fault system ruptured in a major trapdoor faulting event [3-4]. The eruption lasted for 8 days and resulted in ~5 m of caldera deflation. Immediately following the eruption, caldera inflation resumed [4].

In this paper we study the deformation prior to the 2005 eruption, and explain some of the InSAR post-processing and modeling steps in more detail than was possible in our previous studies [6,7]. We will also show an example of the results of the stress-change calculations.

## 2. DEFORMATION DATA

We use both GPS and InSAR data in the deformation modeling. The GPS displacements are described in Ref. [6], and were derived from 5-day averages of daily solutions. The GPS location uncertainties were estimated from the day-to-day repeatability of the station coordinates, resulting in 1-σ displacement errors of 3-16 mm and 14-30 mm for the horizontal and vertical components, respectively.

The InSAR data consist of one descending ERS-1/2 and two descending (IS-2) Envisat interferograms (Fig. 2a-c). One interferogram shows uplift during 12 February 2004 - 27 January 2005. The other two exhibit signals due to inflation as well as faulting on the southern intra-caldera faults on 11 January 1998 and 16 April 2005 (Fig. 2a-b). The uplift contribution in the latter interferogram was removed by subtracting a scaled (×0.59) version of the uplift interferogram (Fig. 2c), and thus assuming that the pattern of uplift was the same during the two time periods. The scalar was estimated from the GPS data [6]. The resulting interferogram should only show deformation due to the 16 April 2005 event (Fig. 2d).

To reduce the large number of InSAR data points, we sub-sampled the InSAR data using quadtree decomposition [10]. The sub-sampling resulted in only 290 and 331 data points for the uplift and 2005 faulting interferograms, respectively, without losing many details of the deformation (Fig. 3).

The InSAR errors were estimated by analyzing the strength and structure of the InSAR noise in non-deforming areas north of the caldera [11]. We selected four areas in the interferograms and estimated

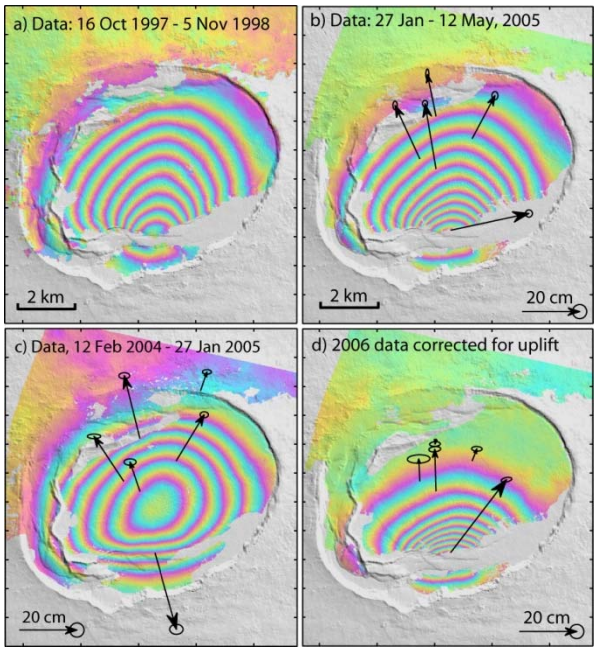


*Figure 2: Unwrapped interferograms (and rewrapped at 10 cm per fringe) showing both uplift and faulting along the southern intra-caldera faults in 1997-98 (a) and in 2005 (b). Uplift observed in 2004-5 (c) was used to eliminate the uplift signal in (b), leaving only deformation due to the 16 April 2005 faulting (d). Results of horizontal continuous GPS measurements in 2004-5 are shown as arrows (95% confidence ellipses).*

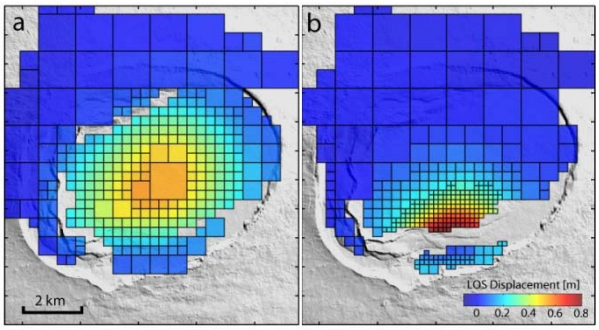


*Figure 3: Sub-sampled versions of the two radar interferograms (Fig. 2c-d) used in the modeling, consisting of 290 and 331 data points.*

the average isotropic covariance structure for the interferograms from the sub-images (Fig. 4). From the covariance structures, the InSAR parts of the data covariance matrices were constructed. As described above, the 2005 faulting data were corrected for uplift, which we can describe as a linear operation: $\mathbf{d^f} = \mathbf{A}\,\mathbf{d^o}$, where $(\mathbf{d^o})^\mathbf{T} = \left[\ (\mathbf{d^{uf}})^\mathbf{T} \quad (\mathbf{d^u})^\mathbf{T}\ \right]$ are the original data sets (Fig. 2b-c) stored in one long column vector and $\mathbf{A}$ is the linear operator $\mathbf{A} = \left[\ \mathbf{I} \quad -0.59\mathbf{I}\ \right]$. Then the covariance matrix for the uplift corrected data $\mathbf{d^f}$ is $\Sigma_d^f = \mathbf{A}\Sigma_d^o\mathbf{A}^\mathbf{T}$ where $\Sigma_d^o$ is a block-diagonal matrix containing the covariance

matrices for both data sets in Fig. 2b-c. The uplift and 2005 faulting data covariance matrices, $\Sigma_d^u$ and $\Sigma_d^f$ therefore both account for spatial correlations in the data and provide a meaningful relative weight between the GPS and InSAR data sets.

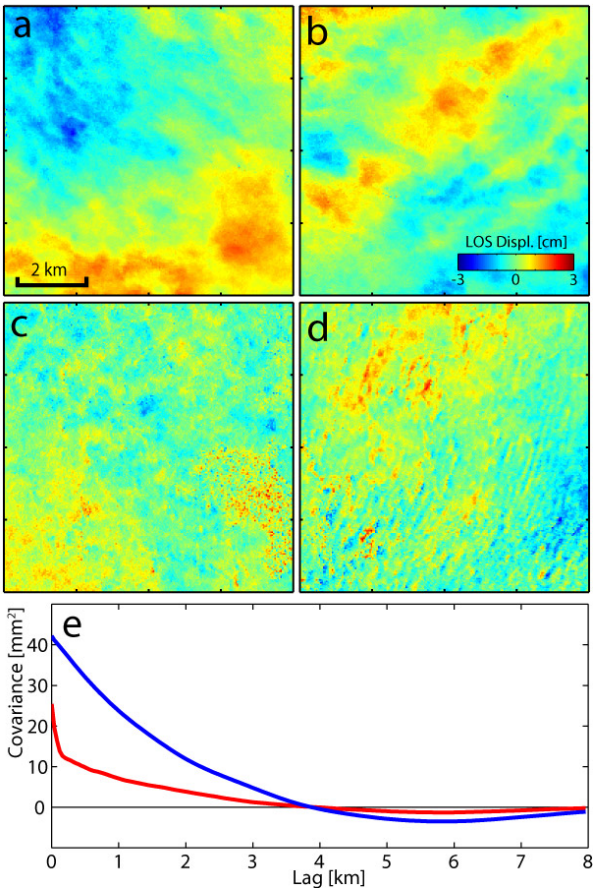


*Figure 4: Unwrapped images from the area north of the caldera exhibiting spatially correlated signal primarily caused by heterogeneities in the atmosphere (displayed as LOS displacement equivalent). (a-b) correspond to the InSAR data in Fig. 2c and (c-d) the data in Fig. 2b. (e) shows the resulting covariance functions for (a-b) in blue and (c-d) in red.*

## 3. DEFORMATION MODELING

We use both GPS and InSAR data of the uplift in 2004-5 (Fig. 2c) to estimate the best-fitting parameters of a horizontal dislocation sill in an elastic half-space [12]. The parameter estimation is carried out in two steps. First the depth and dimensions of a sill with uniform opening were estimated through a non-linear parameter optimization, resulting in a sill-depth of 2.2 km. Then the sill dimensions were expanded to 6 km × 10 km, while its depth was kept at 2.2 km, and variable opening estimated (each cell 0.5 × 0.5 km$^2$) using a non-negative linear least-squares method. The sill opening was subject to smoothing constraints, similar to those used when variable fault slip is estimated from geodetic data [10]. The resulting sill opening has a maximum of about 1.5 m and its shape is elongated along the major axis of the caldera (Fig. 5).

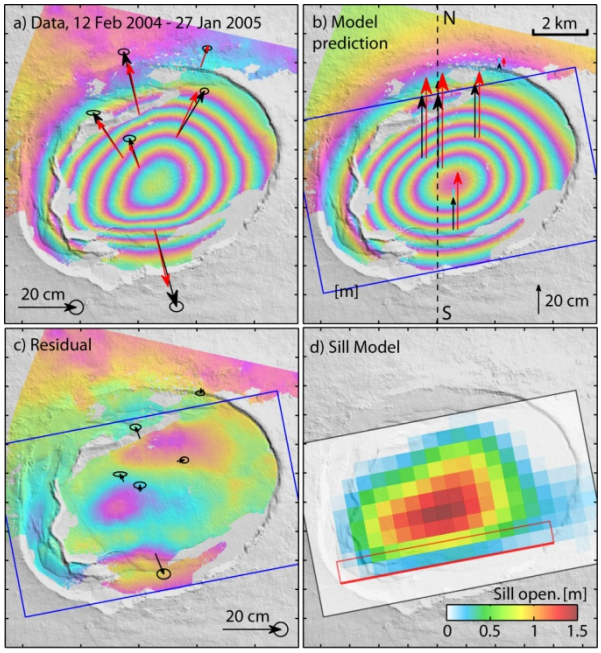


*Figure 5: Observations and modeling of the uplift at Sierra Negra. (a) Same data as in Fig. 2c in comparison with predicted horizontal GPS displacements (red arrows) of the best sill model. (b) InSAR model prediction as well as the observed and predicted vertical GPS displacements. The blue rectangle marks the outer boundaries of the sill model. (c) Residuals between observed and predicted InSAR and horizontal GPS displacements. (d) The best sill model at 2.2 km depth showing up to 1.5 m of opening. Also shown is the surface projection (red rectangle) of the north-dipping trapdoor fault; thicker line marks the surface trace [7].*

Deformation modeling of the 16 April faulting (Fig. 2d) was carried out in a similar way as the sill modeling. First the optimal parameters of a simple rectangular fault with a uniform slip were found, resulting in a steep north-dipping (71°) thrust fault that strikes approximately East-West along the southern intra-caldera faults. We then expanded the dimensions of the fault and solved for variable slip that was subjected to smoothing constraints, but had free-slipping boundary conditions along the upper and lower edges of the fault. The resulting variable slip model has a maximum of 2 m thrust faulting near the bottom of the fault, just above the sill (Fig. 6). More details of the fault modeling can be found in Ref. [6-7].

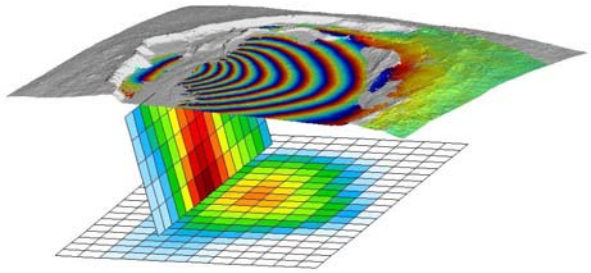

*Figure 6: Perspective view showing the observed deformation 27 Jan. – 12 May 2005 (Fig. 2b) and the modeled sill inflation and thrust faulting. The color-scale is 0-2 m of sill opening or fault slip.*

To estimate the model parameter uncertainties we first add realizations of random correlated noise to the GPS and InSAR data to form multiple synthetic data sets. We then estimate the fault parameters for each of the synthetic data sets and produce a distribution of sill and fault models, from which we can assess the probability distribution of the model parameters. This, however, results in unrealistically low model parameter uncertainties. The reason lays at least in part in a high normalized $\chi^2$ value, which is around 10. This high value indicates that either the data errors are underestimated or the models themselves are too simple. The latter explanation is probably more important as we are using a single planar dislocations an elastic halfspace. To account for the limitations of the model, however, we simply scale the data covariance matrix such that the normalized $\chi^2$ value becomes equal to 1. We then base the multiple random realizations on the scaled version of data covariance matrix. With the resulting distribution of model parameters we can estimate the full posterior model parameter probability distribution, from which we can evaluate correlations between different model parameters and their uncertainties.

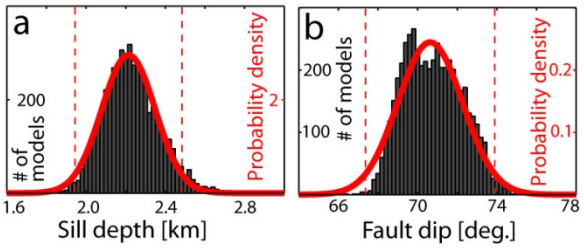


*Figure 7: Histograms showing the distribution of (a) sill-depth and (b) trapdoor fault-dip (to the north) values, as well as the best fit Gaussian probability density function (red). Vertical dashed lines indicate 95% confidence bounds.*

Histograms of the resulting sill depths and fault dips show that they can be reasonably well approximated with a Gaussian distribution (Fig. 7). We therefore assume that the marginal distributions for these two parameters are Gaussian and estimate the best-fitting Gaussian means and standard deviations. The result shows that the best-fit fault is clearly a north-dipping thrust fault with a dip in the range of 67-74° and that the sill lies at 1.9-2.5 km depth, at a 95% confidence level.

## 4. STRESS-CHANGE MODELING

We use the estimated sill model to calculate the stress-changes within an elastic halfspace [12], assuming values for the shear modulus (μ=10 GPa) and Poisson's ratio (ν=0.25). The mean stress change (or pressure change) shows compression above and below the sill, but extension near the peripheries of the sill as well as near the surface directly above the sill (Fig. 8). The directions of the minimum and maximum principal stress-change axes are generally radial, but the plunge of the axes varies both spatially and with depth. At the location of the modeled southern intra-caldera fault, the plunge of the maximum compressional stress axis is about ~40-45° towards the center of the caldera. This plunge is about 25-30° from the estimated 71° dipping fault plane, which is optimal for driving slip on the fault, assuming it has a typical frictional strength. We therefore conclude that sill inflation was the sole trigger of the trapdoor faulting along the southern intra-caldera faults.

The trapdoor faulting causes pressure relief within the sill but compression south of the fault. This tends to inhibit sill growth to the south and would lead to thickening of the sill intrusion north of the fault. More details about the stress-change calculations can be found in Ref. [7].

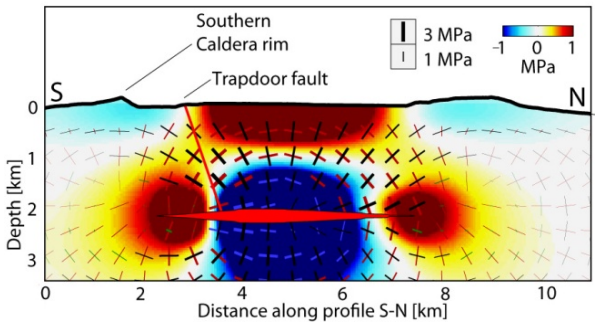


*Figure 8: Cross-section S-N (see Fig. 5b) showing the calculated mean stress increase (extension, red) and decrease (compression, blue) due to the inflating sill at 2.2 km depth. Also shown are the maximum (black bars) and minimum compressional stress-change directions (red and blue bars). The bar thickness indicates half the magnitude of the absolute differential stress-change* $|\Delta\sigma_1 - \Delta\sigma_3|/2$.

## 5. CONCLUSIONS

The observed inflation during 2004-5 can be reproduced using a sill model embedded at 2.2 km depth within an elastic halfspace and with sill opening of up to 1.5 m. The 16 April 2005 trapdoor faulting along the southern intra-caldera faults took place on a steep north-dipping thrust fault with up to 2 m of slip. Calculations of the stress changes caused by the model sill at Sierra Negra show that faulting is encouraged above the peripheries of the sill on inward dipping thrust faults, providing independent evidence for the geometry of the trapdoor faulting that agrees with the dislocation modeling. The trapdoor faulting causes pressure relief within the sill and compression to the south of the fault. This inhibits sill growth to the south and causes thickening of the sill north of the fault.

## 6. ACKNOWLEDGEMENTS

The satellite radar data were provided by the European Space Agency through Category-1 project #3493. This work was supported by NSF grants EAR-0207605, 0538205, and 0004067.

## 7. REFERENCES

1. Reynolds, R.W., Geist, D. & Kurz, M.D. (1995). Physical volcanology and structural development of Sierra Negra volcano, Isabela island, Galápagos archipelago, *GSA Bull.* 107, 1398-1410.
2. Jónsson, S., Zebker, H. & Amelung, F. (2005). On trapdoor faulting at Sierra Negra volcano, Galápagos. *J. Volcanol. Geotherm. Res.* 144, 59-71.
3. Yun S.-H., Zebker, H., Segall, P., Hooper, A. & Poland, M. (2006a). 2005 Eruption at Sierra Negra volcano unveiled by InSAR observations. *EOS Trans. AGU Fall Meet. Assem. Suppl.* 87(52), Abstract G52A-01.
4. Geist, D.J., Harpp, K.S., Naumann, T.R., Poland, M., Chadwick, Jr., W.W., Hall, M. & Rader, E. (2007). The 2005 eruption of Sierra Negra volcano, Galápagos, Ecuador. *Bull. Volcanol.*, doi 10.1007/s00445-007-0160-3.
5. Amelung, F., Jónsson, S., Zebker, H. & Segall, P. (2000). Widespread uplift and 'trapdoor' faulting on Galápagos volcanoes observed with radar interferometry. *Nature* 407, 993-996.
6. Chadwick Jr., W.W., Geist, D.J., Jónsson, S., Poland, M., Johnson, D.J. & Meertens, C.M. (2006). A volcano bursting at the seems: Inflation, faulting, and eruption at Sierra Negra volcano, Galapagos. *Geology* 34(12), 1025-1028.
7. Jónsson, S. (2007). Stress interaction between magma accumulation and trapdoor faulting on Sierra Negra volcano, Galápagos. *Tectonophysics* (submitted).
8. GCMT: The Global Centroid-Moment-Tensor project: http://www.globalcmt.org
9. NEIC: National Earthquake Information Center, U.S. Geological Survey: http://neic.usgs.gov
10. Jónsson, S., Zebker, H., Segall, P. & Amelung, F. (2002). Fault Slip Distribution of the 1999 Mw7.1 Hector Mine Earthquake, California, estimated from Satellite Radar and GPS Measurements. *Bull. Seismol. Soc. Am.* 92, 1377-1389.
11. Sudhaus, H. & Jónsson, S. (2007). Improved source imaging of the Kleifarvatn earthquake, Iceland, through a combined use of ascending and descending InSAR data. In: *Proc. Envisat Symp. Montreux.* European Space Agency.
12. Okada, Y. (1992). Internal deformation due to shear and tensile faults in a half-space. *Bull. Seismol. Soc. Am.* 82, 1018-1040.